THE JOURNAL OF BIOLOGICAL CHEMISTRY VOL. 283, NO. 47, pp. 32900–32912, November 21, 2008

Molecular Recognition of Corticotropin-releasing Factor by Its G-protein-coupled Receptor CRFR1*[S]

Received for publication, July 28, 2008, and in revised form, September 17, 2008 Published, JBC Papers in Press, September 17, 2008, DOI 10.1074/jbc.M805749200

Augen A. Pioszak[1], **Naomi R. Parker, Kelly Suino-Powell, and H. Eric Xu**[2]

From the Laboratory of Structural Sciences, Van Andel Research Institute, Grand Rapids, Michigan 49503

The bimolecular interaction between corticotropin-releasing factor (CRF), a neuropeptide, and its type 1 receptor (CRFR1), a class B G-protein-coupled receptor (GPCR), is crucial for activation of the hypothalamic-pituitary-adrenal axis in response to stress, and has been a target of intense drug design for the treatment of anxiety, depression, and related disorders. As a class B GPCR, CRFR1 contains an N-terminal extracellular domain (ECD) that provides the primary ligand binding determinants. Here we present three crystal structures of the human CRFR1 ECD, one in a ligand-free form and two in distinct CRF-bound states. The CRFR1 ECD adopts the α-β-βα fold observed for other class B GPCR ECDs, but the N-terminal α-helix is significantly shorter and does not contact CRF. CRF adopts a continuous α-helix that docks in a hydrophobic surface of the ECD that is distinct from the peptide-binding site of other class B GPCRs, thereby providing a basis for the specificity of ligand recognition between CRFR1 and other class B GPCRs. The binding of CRF is accompanied by clamp-like conformational changes of two loops of the receptor that anchor the CRF C terminus, including the C-terminal amide group. These structural studies provide a molecular framework for understanding peptide binding and specificity by the CRF receptors as well as a template for designing potent and selective CRFR1 antagonists for therapeutic applications.

Corticotropin-releasing factor (CRF)[3] is a 41-amino acid, C-terminally amidated neuropeptide originally isolated from sheep hypothalami based on its ability to stimulate secretion of adrenocorticotropin from pituitary cells (1). Several other CRF-related peptides have since been identified, including the urocortins (Ucn) I, II, and III in mammals (2–5). Extensive studies over the last nearly 3 decades have highlighted the critical roles that CRF family peptides play in coordinating endocrine, autonomic, and behavioral responses to stress (reviewed in Refs. 6, 7). The CRF family of peptides exert their effects through the binding and activation of two paralogous cell surface G-protein-coupled receptors (GPCRs), CRFR1 (8) and CRFR2 (9–11). CRF binds to both receptors but with higher affinity for CRFR1. UcnI binds equally well to both receptors, whereas UcnII and UcnIII are selective for CRFR2. CRF is the primary regulator of central stress responses; its binding to CRFR1 on the surface of pituitary corticotrope cells activates the hypothalamic-pituitary-adrenal axis. Consequently, there has been enormous interest in the therapeutic potential of CRFR1-selective antagonists for the treatment of anxiety, depression, and related disorders (reviewed in Refs. 7, 12).

The CRF receptors belong to the class B/Secretin family of GPCRs (13), whose members include receptors for parathyroid hormone, calcitonin, glucagon, glucagon-like peptides, and other therapeutically important peptides. In addition to a 7-transmembrane helical domain common to all GPCRs, class B receptors have an N-terminal extracellular domain (ECD) of roughly 100–160 amino acids that contains three conserved disulfide bonds. Ligand binding and activation of the receptors are thought to occur by a two-domain model (reviewed in Ref. 14). The C-terminal portion of the peptide ligand provides the primary receptor binding determinants and interacts with the ECD to bring the N-terminal portion of the peptide in proximity to the 7-transmembrane helical domain where it activates the receptor. Many studies support the two-domain model for CRFR1. Chimeric receptor studies indicated that the CRFR1 ECD provides the primary ligand binding determinants (15–17). Moreover, recombinant expression and purification of the isolated ECD confirmed its ability to bind ligands (18, 19). A chimeric receptor in which the ECD of CRFR1 was replaced with the 16 N-terminal residues of CRF exhibited constitutive activation (20), and the isolated 7-transmembrane helical domain was activated by agonist peptides, albeit with reduced potency (21). It has long been recognized that the C-terminal amide moiety of CRF and a helical conformation of the peptide are critical for high affinity binding to the receptor (1, 22).

* This work was supported, in whole or in part, by National Institutes of Health Grants DK071662, DK066202, and HL089301. This work was also supported by The Jay and Betty Van Andel Foundation and Michigan Economic Development Corporation Grant 085P1000817. The costs of publication of this article were defrayed in part by the payment of page charges. This article must therefore be hereby marked "*advertisement*" in accordance with 18 U.S.C. Section 1734 solely to indicate this fact.

The atomic coordinates and structure factors (codes 3EHS, 3EHU, and 3EHT) have been deposited in the Protein Data Bank, Research Collaboratory for Structural Bioinformatics, Rutgers University, New Brunswick, NJ (http://www.rcsb.org/).

[S] The on-line version of this article (available at http://www.jbc.org) contains supplemental Figs. S1–S4 and Table S1.

[1] To whom correspondence may be addressed: Laboratory of Structural Sciences, Van Andel Research Institute, 333 Bostwick Ave. NE, Grand Rapids, MI 49503. E-mail: augie.pioszak@vai.org

[2] To whom correspondence may be addressed. E-mail: eric.xu@vai.org.

[3] The abbreviations used are: CRF, corticotropin releasing factor; CRFR, CRF receptor; Ucn, urocortin; PTH, parathyroid hormone; PTH1R, PTH receptor type 1; GIP, glucose-dependent insulinotropic peptide; GIPR, GIP receptor; GLP1R, glucagon-like peptide 1 receptor; GPCR, G-protein-coupled receptor; PDB, Protein Data Bank; MBP, maltose-binding protein; ECD, extracellular domain; MOPS, 4-morpholinepropanesulfonic acid; BisTris, 2-[bis(2-hydroxyethyl)amino]-2-(hydroxymethyl)propane-1,3-diol; Tricine, *N*-[2-hydroxy-1,1-bis(hydroxymethyl)ethyl]glycine; SCR, short consensus repeat; MR, molecular replacement; PEG, polyethylene glycol; TLS, translation, libration, screw rotation.

Truncation of N-terminal residues of CRF creates competitive antagonists (22). Numerous such CRF analogs have been synthesized that display varying potency and selectivity for CRFR1 and CRFR2 (23–25). Astressin, a high affinity antagonist that binds both receptors, is a modified version of CRF-(12–41)-NH_2 constrained by a helix-stabilizing lactam bridge (26). Potent astressin-like antagonists as short as fragments 27–41 or 30–41 have also been reported (27, 28).

Recently, considerable insight into the ligand binding mechanisms of class B GPCRs has been gained from several reports of ECD·peptide complex structures determined by NMR or x-ray crystallographic methods. The NMR solution structure of astressin bound to the mouse CRFR2β ECD showed that the ECD consists of two antiparallel β-sheets, each with two β-strands that are held together by the conserved disulfide bonds. The arrangement of the CRFR2β ECD resembles the short consensus repeat (SCR) fold that is also present in the Ig family of proteins (29). The astressin 27–41-amino acid fragment forms an amphipathic α-helix that interacts with a hydrophobic surface of the ECD at the interface of three loop regions. Subsequent reports described the structures of pituitary adenylate cyclase-activating polypeptide, glucose-dependent insulinotropic peptide (GIP), exendin-4, and parathyroid hormone (PTH) in complex with their cognate receptor ECDs (30–33). No structure of the CRFR1 ECD has been reported to date, although the conformation of a short astressin-like antagonist when bound to the CRFR1 ECD was determined by NMR methods (34). A high resolution structure of the CRF·CRFR1 ECD complex is required to understand how the endogenous ligand binds the receptor and will provide insight into ligand selectivity and aid rational drug design targeting CRFR1.

We previously reported a general methodology for the expression, purification, and crystallization of the N-terminal ECD of class B GPCRs and demonstrated its applicability for the PTH1R ECD (31). The PTH1R ECD was expressed as a fusion to bacterial maltose-binding protein (MBP) in the oxidizing cytoplasm of an *Escherichia coli trxB gor* host to facilitate disulfide bond formation, and the fusion protein was purified and subjected to *in vitro* disulfide shuffling in a redox buffer to maximize the yield of properly folded protein. The MBP tag facilitated crystallization of the PTH1R ECD by providing a large surface area for crystal contacts. Here we show that the methodology is applicable to the ECD of human CRFR1, and we describe the crystal structures of the CRFR1 ECD in the ligand-free and CRF-bound states, discuss conformational changes associated with CRF binding, and compare the CRFR1 ECD structures to those of the mouse CRFR2β ECD and other class B GPCR ECDs.

EXPERIMENTAL PROCEDURES

Molecular Biology Methods—The plasmid for expression of the human CRFR1 ECD as a fusion to bacterial maltose-binding protein (MBP) was constructed as described previously for the PTH1R ECD (31). Briefly, a DNA fragment corresponding to residues 24–119 of human CRFR1 (excluding the native signal peptide residues 1–23) was PCR-amplified with a C-terminal six histidine residue tag from a CRFR1 cDNA clone obtained from the UMR cDNA resource center. After digestion with EcoRI and NotI restriction endonucleases, the fragment was ligated into an isopropyl 1-thio-β-D-galactopyranoside-inducible, T7 promoter-driven, bacterial expression vector that permits co-expression of the MBP-CRFR1-ECD-H_6 protein with the bacterial disulfide isomerase/chaperone DsbC as described previously (31). Single amino acid substitutions in MBP were introduced by site-directed mutagenesis of the expression vector using the Stratagene Quikchange kit according to the manufacturer's directions. All plasmid constructs were verified by DNA sequencing.

Protein Expression and Purification—The CRFR1 ECD was expressed as a fusion protein with maltose-binding protein (MBP) at its N terminus and a His_6 tag at its C terminus in the *E. coli* strain Origami B (DE3) (Novagen) as described previously (31). The purification protocol was as described previously for the MBP-PTH1R ECD fusion protein (31), with the exceptions noted below. First, the fusion protein was purified by affinity chromatography via the His_6 and MBP tags on nickel-chelating Sepharose resin (GE Healthcare) followed by amylose resin (New England Biolabs). Second, *in vitro* disulfide shuffling in a 1 mM GSH, 1 mM GSSG redox buffer was performed to increase the yield of properly folded protein. Third, Superdex 200 gel filtration (GE Healthcare) chromatography was used to separate the properly folded and misfolded protein. Finally, the protein was subjected to QFF anion exchange (GE Healthcare) chromatography. The disulfide shuffling reaction mixture was incubated at 13 °C overnight and did not require the addition of purified DsbC, thus permitting application of the shuffling reaction mixture to the gel filtration column without the need to first remove DsbC. Proteins with site-specific amino acid substitutions in MBP were purified in the same manner as wild type, with the exception of the MBP(A326E)-CRFR1 ECD protein for which the amylose step was omitted. (The numbering of MBP residues is based on our synthetic construct.) Protein concentrations were determined by the method of Bradford (35) with bovine serum albumin as the standard. Native gel electrophoresis was performed as described (31).

Peptide Synthesis—Peptides were custom-synthesized and high pressure liquid chromatography-purified by SynBioSci (Livermore, CA). The concentrations of stock solutions were determined based on the theoretical peptide content reported by SynBioSci. Peptide integrity was internally verified by analysis of aliquots by Tris-Tricine SDS-PAGE and mass spectrometry. All peptides contain a C-terminal amide group unless indicated otherwise.

Peptide Binding Assay—Association of CRF with MBP-CRFR1-ECD was determined by an AlphaScreen™ luminescent proximity assay (PerkinElmer Life Sciences) using a histidine detection kit similar to a previously described assay (31). The reaction mixtures contained 5 μg/ml each of streptavidin-coated donor beads and nickel-chelate-coated acceptor beads, and biotin-Gly-Gly-Gly-CRF-(12–41)-NH_2 and MBP-CRFR1-ECD-H_6 as indicated in a buffer of 50 mM MOPS, pH 7.4, 100 mM NaCl, and 0.1 mg/ml bovine serum albumin. Equilibrium was achieved after incubation at 22 °C for 4.5 h, at which point signal recording was performed in a 384-well microplate with an Envision 2104 plate reader (PerkinElmer Life Sciences). For

competition experiments, unlabeled competitor peptides were added at time 0, and the reactions were allowed to reach equilibrium before signal recording. Nonlinear regression as implemented in Prism 5.0 (GraphPad Software, San Diego) was used to fit the data to a variable slope dose-response inhibition equation for determination of IC_{50} values. Control experiments to ensure that inhibition of the signal by unlabeled peptides was specific were carried out using a biotin-Gly_6-His_6 peptide (25 nM) in place of the biotinylated CRF-(12–41) and MBP-CRFR1-ECD-H_6.

Crystallization and Data Collection—Crystal growth was carried out at 20 °C. For ligand-free MBP-CRFR1-ECD-H_6, a protein sample in 10 mM Tris-HCl, pH 7.5, 1 mM EDTA, and 1 mM maltose was concentrated to ~14 mg/ml using an Amicon ultracentrifugal filter device (Millipore) with a molecular mass cutoff of 3 kDa. For the receptor·peptide complexes, a protein sample in 10 mM Tris-HCl, pH 7.5, 50 mM NaCl, 1 mM EDTA, and 1 mM maltose was complexed with a synthetic CRF fragment at a molar ratio of 1:1.2 (protein:peptide) and incubated on ice for 30 min, after which the mixture was concentrated to ~18 mg/ml as above. Initial crystal screening utilized kits from Hampton Research and an Art Robbins Instruments Phoenix robot. Optimizations of the initial hits were performed manually using the hanging drop vapor diffusion method with drops containing equal volumes of protein and reservoir solution. Large, bipyramidal crystals of the ligand-free protein (crystal form I) were grown over a reservoir solution of 0.1 M sodium acetate, pH 4.7, 1.8 M NaCl, and 30% (w/v) sucrose. For crystallization of the receptor·ligand complexes, MBP-CRFR1 ECD fusion proteins containing the site-specific alterations F94E or A326E in MBP were used to prevent an unfavorable crystal packing interaction with the CRFR1 ECD that prevented crystallization of the wild-type fusion protein in complex with CRF. Plate-shaped crystals of the CRF-(22–41)-bound receptor (crystal form II) were grown with the A326E-altered fusion protein over a reservoir of 0.1 M BisTris, pH 6.75, 0.1 M $CaCl_2$, 22% (v/v) polyethylene glycol (PEG) monomethyl ether 550, and 3% (v/v) *tert*-butyl alcohol. Microseeding was used to obtain single plate crystals for crystal form II. Bipyramidal crystals of the CRF-(27–41)-bound receptor (crystal form III) were grown with the F94E-altered fusion protein over a reservoir of 0.1 M BisTris, pH 6.25, 0.2 M Li_2SO_4, and 20% (v/v) PEG 3350. All crystals appeared and completed growth within a few days.

The crystals were flash-cooled in cryoprotectant solution by plunging into liquid nitrogen. Crystal form I was suitably cryoprotected in its mother liquor. For crystal form II, the PEG monomethyl ether 550 concentration was raised to 31% by vapor diffusion overnight. For crystal form III, the PEG 3350 concentration was raised to 28% by serial transfer of the crystal into solutions of increasing PEG concentration. Native diffraction data sets were collected from single crystals, with the data for form I and form III crystals collected at beamline 21-ID-D of the Advanced Photon Source (Argonne, IL), and data for crystal form II collected at beamline 21-ID-F. The datasets were processed and scaled with the HKL2000 package (36). The data collection statistics are summarized in Table 1.

Structure Solution and Refinement—The CCP4 suite was used to convert the Scalepack intensities to structure factor amplitudes and flag 5% of the reflections for cross-validation (37). All three structures were solved by the molecular replacement (MR) method using Phaser (38). The ligand-free structure (crystal form I) was solved using separate search models for MBP and a model of the PTH1R ECD with the N-terminal α-helix removed. The coordinates used were from our previously reported structure of MBP-PTH1R-ECD, PDB code 3C4M (31). The ligand-bound structures (crystal forms II and III) were solved using separate search models for MBP and the CRFR1 ECD from the ligand-free structure (this work). The MR solutions were subjected to restrained refinement with Refmac5 (39). The $2F_o - F_c$ and $F_o - F_c$ electron density maps from the refined MR solutions were all sufficiently clear as to obviate the need for density modification. The MR solutions were verified by clear electron density for the maltose molecule, which was not included in the MR search models, as well as clear density for the peptide ligand for crystal forms II and III. Iterative cycles of manual rebuilding in O (40) and restrained refinement with Refmac5 were used to finish the models. Noncrystallographic symmetry restraints were applied for crystal form II in the initial stages and gradually released as the model improved. TLS refinement was included for all three structures (41). Two TLS groups corresponding to protein domains were used for crystal form I as follows: one for the MBP·maltose complex, and the other for the CRFR1 ECD. Six TLS groups were used for crystal form II as follows: one for each of the two MBP·maltose complexes, one for each of the two CRFR1 ECDs, and one for each of the two CRF peptides. Because of the low resolution of crystal form III, a single TLS group comprising the contents of the asymmetric unit was used. Water molecules were added to the form II structure using the ARP feature of CCP4 (37) in combination with Refmac5. Structure validation was performed with Procheck (42). The refinement statistics are summarized in Table 1.

Amino Acid Sequence Alignments, Structure Analysis, and Figure Preparation—Amino acid sequence alignments were performed with ClustalW (43) and the results displayed with ESpript (44). Structural alignments were performed using the align command in PyMol (45), with the alignments based on the core SCR fold of the ECD excluding the N-terminal α-helix, loop 1, and loop 2. Accessible surface area calculations were performed with the program Areaimol in the CCP4 suite (37). Structure figures were prepared with PyMol. "Shake" omit electron density maps were used to reduce model bias for displaying ligand density in Figs. 3 and 4. The coordinates of the final refined model were randomly shifted by ~0.3 Å using Moleman (46), and the peptide ligands were omitted. The resulting model was subjected to 5–10 cycles of restrained refinement with Refmac5, and maps were calculated from the refined omit model.

RESULTS

Expression and Purification of the CRFR1 ECD as an MBP Fusion Protein That Readily Crystallizes—The ECD of human CRFR1 (residues 24–119) was expressed in the oxidizing cytoplasm of an *E. coli trxB gor* host strain as a soluble fusion protein with MBP at its N terminus and a His_6 tag at its C terminus. The MBP-CRFR1-ECD-H_6 fusion protein was purified using the methodology we developed for class B GPCR ECDs as demon-

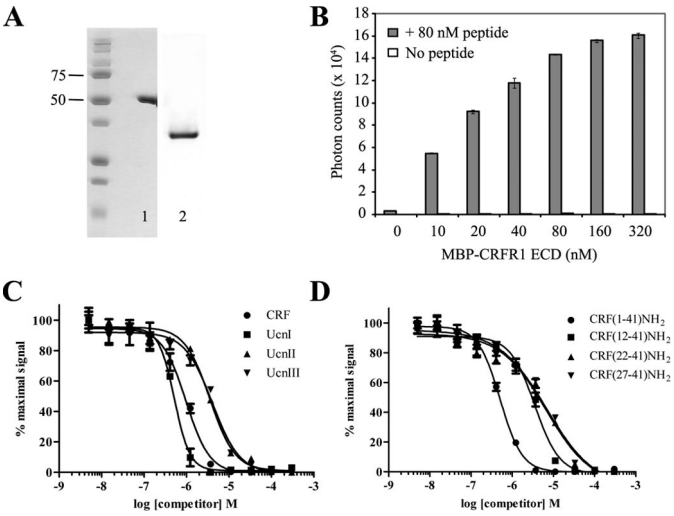

FIGURE 1. **Purification and function of the MBP-CRFR1-ECD-H_6 fusion protein.** *A*, analysis of the purified fusion protein by nonreducing SDS-PAGE (*lane 1*) and nondenaturing (native)-PAGE (*lane 2*). Molecular mass markers are shown in kDa. The gels were stained with Coomassie Brilliant Blue R-250. *B*, AlphaScreen assay for association of N-terminally biotinylated CRF-(12–41)-NH_2 with MBP-CRFR1-ECD-H_6. *C*, competition AlphaScreen assay assessing the ability of unlabeled, full-length CRF family peptides to inhibit the association of biotin-CRF-(12–41)-NH_2 (25 nM) with MBP-CRFR1-ECD-H_6 (25 nM). The IC_{50} values for CRF, UcnI, UcnII, and UcnIII were 1.0, 0.5, 3.6, and 4.1 μM, respectively. *D*, competition AlphaScreen assay assessing the ability of unlabeled, truncated CRF peptides to inhibit the association of biotin-CRF-(12–41)-NH_2 (25 nM) with MBP-CRFR1-ECD-H_6 (25 nM). The IC_{50} values for CRF-(1–41), CRF-(12–41), CRF-(22–41), and CRF-(27–41) were 0.5, 3.5, 6.6, and 6.8 μM, respectively. The AlphaScreen results represent the average of duplicate reactions.

strated previously for the PTH1R ECD (31). A key feature of the method involves incubating the affinity chromatography-purified fusion protein in a GSH/GSSG redox buffer to promote shuffling of the disulfide bonds and increase the yield of properly folded protein. Notably, in contrast to the protocol for MBP-PTH1R-ECD, the shuffling of disulfide bonds within the CRFR1 ECD did not require the bacterial disulfide isomerase/chaperone DsbC (data not shown). This simplified the purification of MBP-CRFR1-ECD as compared with MBP-PTH1R-ECD. The disulfide shuffling reaction mixture eluted as two peaks from a gel filtration column, one at the void volume and the other at a volume corresponding to the monomer (data not shown). The monomeric sample exhibited a single, distinct band in nonreducing native or SDS-denaturing gels (Fig. 1*A*), demonstrating its conformational homogeneity and purity. The yield of the final purified protein was 5–10 mg/liter of bacterial culture.

The ability of the MBP-CRFR1-ECD fusion protein to bind to CRF was confirmed by an AlphaScreen assay (PerkinElmer Life Sciences). In this assay, N-terminally biotinylated CRF-(12–41) was attached to streptavidin-coated donor beads, and the MBP-CRFR1-ECD-H_6 fusion protein was attached to nickel-chelate-coated acceptor beads via the His_6 tag. Association of the CRF peptide with the fusion protein resulted in a dose-dependent binding signal (Fig. 1*B*). Competition experiments with unlabeled, full-length CRF family peptides indicated that the CRFR1 ECD displayed selectivity for CRF and UcnI over UcnII and UcnIII (Fig. 1*C*). The affinity of CRF for the CRFR1 ECD as estimated by the IC_{50} value was in the 500–1000 nM range (Fig. 1, *C* and *D*), similar to the affinity of other peptide hormones for their cognate class B GPCR ECDs (30, 31). We also examined the ability of truncated versions of CRF to compete with the interaction (Fig. 1*D*). CRF-(12–41), CRF-(22–41), and CRF-(27–41) displayed ~10-fold lower estimated affinities (low micromolar range) for the CRFR1 ECD than the full-length peptide, probably because of a loss of helical propensity by removing the N-terminal residues (26). These results demonstrate that the CRFR1 ECD is properly folded and is capable of binding short CRF peptides that do not contain α-helical stabilizing lactam bridges, albeit with low affinity. Importantly, the MBP-CRFR1-ECD fusion protein was crystallized in a ligand-free form, and in two distinct CRF-bound states (data not shown).

Structure of the CRFR1 ECD in the Absence of Ligand—Crystals of the ligand-free MBP-CRFR1-ECD fusion protein formed in the tetragonal $P4_12_12$ space group with one molecule in each asymmetric unit (crystal form I). The structure was solved by molecular replacement (MR) and refined to an *R* factor of 20.7% (R_{free} factor of 24.0%) at 2.75 Å resolution (Table 1). The moderate diffraction resolution of the crystal was presumably because of the high solvent content of ~72%. However, excellent electron density was observed for all CRFR1 ECD residues except 109–119 and the His_6 tag which were excluded from the final model. The CRFR1 ECD fold consists of a short N-terminal α-helix followed by two anti-parallel β-sheets each with two β-strands, and a short C-terminal α-helix (Fig. 2*A*). The secondary structure elements are arranged in three layers (α-helix 1, β-sheet 1, β-sheet 2/α-helix 2) that are held together by the three conserved disulfide bonds. The two β-sheets form the short consensus repeat (SCR) fold that has been observed in all class B GPCR ECD structures published to date (29–33).

The core of the CRFR1 ECD is packed with residues that are conserved among all 15 human class B GPCR ECDs (Fig. 2*B*). The six invariant cysteine residues form the three conserved disulfide bonds Cys^{30}–Cys^{54}, Cys^{44}–Cys^{87}, and Cys^{68}–Cys^{102}. The aliphatic side chain of Arg^{85} is sandwiched between the invariant tryptophan residues Trp^{55} and Trp^{93}, extending the hydrophobic core of the ECD from the Cys^{44}–Cys^{87}disulfide at the left to Tyr^{99}, the Cys^{68}–Cys^{102} disulfide, and Pro^{69} at the right. The invariant aspartate Asp^{49} stabilizes the $\beta1$-$\beta2$ hairpin loop by forming hydrogen bonds with the indole nitrogen of Trp^{55}, the hydroxyl group of Tyr^{99}, and the backbone amide nitrogens of Ile^{51} and Thr^{53}. The same packing interactions of these conserved residues are observed in all crystal structures of class B GPCR ECDs solved to date (30–32). We see no evidence for a salt bridge between Arg^{85} and Asp^{49} as proposed for the equivalent residues in the mCRFR2β ECD (29, 47).

Three key differences are observed in the overall fold of the hCRFR1 ECD as compared with the mCRFR2β ECD (29). First, the N-terminal helix was not observed in the NMR solution structure of the mCRFR2β ECD (Fig. 2*C*). Our observation of an N-terminal helix is consistent with other class B GPCR ECD structures (30–33), suggesting the N-terminal helix is a common feature. Unlike other class B GPCR ECDs, the CRFR1 N-terminal helix is short and does not make direct contacts with the $\beta3$-$\beta4$ loop (loop 2), thus permitting flexibility in loop 2 that is not observed for PTH1R, GIPR, or GLP1R. Second, the

TABLE 1

Data collection and refinement statistics

The following abbreviations are used: APS, advanced photon source; r.m.s., root mean square; ASU, asymmetric unit.

Crystal form	I, ligand-free	II, CRF-(22–41)-NH_2-bound	III, CRF-(27–41)-NH_2-bound
Data collection			
Beamline	APS 21-ID-D	APS 21-ID-F	APS 21-ID-D
Space group	$P4_12_12$	P1	$P4_12_12$
a, *b*, *c*	112.02, 112.02, 145.79 Å	49.20, 63.48, 85.88 Å	112.92, 112.92, 158.17 Å
α, β, γ	90.0, 90.0, 90.0°	99.75, 106.28, 101.67°	90.0, 90.0, 90.0°
Resolution range	50.00–2.75 Å (2.85–2.75 Å)[a]	50.00–1.96 Å (2.03–1.96 Å)	50.00–3.40 Å (3.52–3.40 Å)
Wavelength	0.97872 Å	0.97872 Å	0.99999 Å
No. of observations	335,781	217,545	100,651
Unique reflections	24,253	64,919	14,697
Completeness	98.4% (90.2%)	94.7% (75.2%)	99.4% (97.2%)
Redundancy	13.8	3.4	6.8
I/σ	33.26 (2.99)	13.49 (2.32)	20.81 (1.88)
R_{merge}[b]	5.9% (57.3%)	11.3% (33.7%)	8.5% (73.9%)
Mosaicity	0.441°	0.909°	0.623°
Refinement			
Resolution range	50.00–2.76	39.50–1.96	50.00–3.40
No. of reflections (total/test)	22,995/1238	61,357/3254	13,897/739
R_{cryst}[c]/R_{free}[d]	20.7%/24.0%	20.9%/25.6%	21.8%/25.2%
MBP-ECD molecules/ASU	1	2	1
No. of TLS groups	2	6	1
Mean *B* value	111.60 Å^2	32.13 Å^2	156.49 Å^2
No. of protein atoms	3539	7044	3586
No. of water atoms	6	450	0
No. of heterogen atoms	23 (1 maltose molecule)	90 (2 maltose, 2 calcium, 2 BisTris, and 2 PEG molecules)	23 (1 maltose molecule)
r.m.s. bond length deviation	0.011 Å	0.012 Å	0.006 Å
r.m.s. bond angle deviation	1.233°	1.285°	0.997°
Ramachandran plot, % residues in[e]			
Most favored	91.9	92.2	89.7
Additional allowed	7.6	7.6	9.5
Generously allowed	0.5	0.3	0.8
Disallowed	0	0	0

[a] Values in parentheses are for the highest resolution shell.
[b] $R_{merge} = \Sigma|I - \langle I\rangle| > |/\Sigma|I|$, where I is the intensity measurement for a given reflection, and $\langle I\rangle$ is the average intensity for multiple measurements of the reflection.
[c] $R_{cryst} = \Sigma(|F_o| - K|F_c|)/\Sigma|F_o|$.
[c] R_{free} was calculated using a randomly selected 5% test set of the total reflections that was omitted from the refinement.
[e] Data were as defined in Procheck (42).

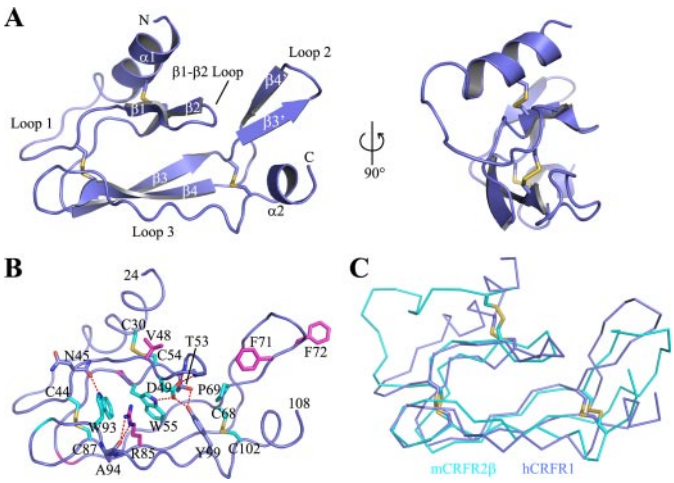

FIGURE 2. **Structure of the ligand-free CRFR1 ECD at 2.75 Å resolution.** *A*, two views of a ribbon diagram showing the CRFR1 ECD (crystal form I) with secondary structure elements labeled. The three disulfide bonds are depicted as *sticks*. MBP is not shown for clarity. *B*, residues that stabilize the SCR fold of the CRFR1 ECD. Selected side chains are shown as *sticks* with their carbon atoms colored according to amino acid sequence conservation among the 15 human class B GPCR ECDs. *Cyan* indicates invariant residues; *magenta* indicates conservative substitutions, and *slate blue* indicates nonconserved residues. Hydrogen bonds are depicted as *red dashes*. *C*, alignment of the crystal structure of the ligand-free hCRFR1 ECD with the NMR solution structure of the ligand-free mCRFR2β ECD (PDB code 2JNC). C-α backbone traces are shown with CRFR1 colored *slate blue* and CRFR2β colored *cyan*.

conformation of loop 2 differs dramatically from that observed for the mCRFR2β ECD (Fig. 2*C*). Loop 2 contains two additional β-strands (noted as $\beta3'$ and $\beta4'$), which form a tight β-hairpin loop. The significance of this structural feature is not clear, but it is most likely because of constraints imposed by extensive crystal packing interactions with a symmetry-related MBP molecule (supplemental Fig. S1). Third, similar to the PTH1R ECD structure, the CRFR1 ECD contains a short helix near its C terminus that is not observed in the NMR structure. The existence of both an N-terminal and a short C-terminal helix in the CRFR1 ECD suggests that all class B GPCR ECDs share a common α-β-$\beta\alpha$ fold beyond the conserved SCR core.

Structural Basis for CRF Binding to the CRFR1 ECD—Initial attempts to crystallize the wild-type MBP-CRFR1-ECD fusion protein in complex with CRF peptides resulted in crystals of bi-pyramidal morphology, similar to the ligand-free crystal form. In two separate cases, we were able to collect diffraction data to ~3.0 Å resolution and solve the structure, only to find that the ligand was absent (data not shown). We hypothesized that the extensive crystal packing interaction involving loop 2 prevented crystallization of the ligand-bound protein (supplemental Fig. S1). Indeed, previous chimeric receptor studies (15, 17) and the NMR solution structure of the astressin-bound mCRFR2β ECD (29) indicated that loop 2 is involved in ligand binding. Thus, we altered MBP residues at the crystal packing interface (F94E or A326E), but we kept the CRFR1 ECD intact with the goal of blocking the interaction with loop 2 (supple-

mental Fig. S1). The MBP-CRFR1-ECD-H_6 fusion proteins containing either F94E or A326E MBP were expressed and purified similar to the wild-type protein for crystallization.

The MBP (A326E)-CRFR1-ECD-H_6 fusion protein bound to a synthetic CRF fragment (residues 22–41) was crystallized in the triclinic P1 space group with two MBP-CRFR1-ECD·CRF complexes in each asymmetric unit (crystal form II). The structure was solved by MR and refined to a *R* factor of 20.9% (R_{free} factor of 25.6%) at 1.96 Å resolution (Table 1). Importantly, the A326E alteration in MBP permitted loop 2 of the CRFR1 ECD to assume a conformation unhindered by packing constraints (supplemental Fig. S2). The CRF peptide was present with electron density observed for residues 26′–41′ (Fig. 3, *A* and *B*). (Peptide residues are denoted with a prime to distinguish them from protein residues.) The electron density map was well defined for much of the CRFR1 ECD, but it was somewhat weak for α1, loop1, and loop 2 (supplemental Fig. S3). ECD residues 24–26, 105–119, and the His_6 tag were excluded from the final model because of disorder. In addition, the side chains of CRF residues $Gln^{26′}$ and $Gln^{29′}$, and ECD residues Phe^{71}, Tyr^{73}, and Arg^{76} of loop 2 were trimmed back to their β-carbon atoms because of poor electron density. The two ECD·CRF complexes are quite similar as indicated by the root mean square deviation of their C-α atom positions of 0.209 Å; thus, we confine our description to the complex between ECD molecule B and CRF molecule D, which have lower average *B* factors than the other complex (supplemental Table S1). The average *B* factors of the peptide are only slightly higher than those of the ECD.

CRF forms a relatively straight, continuous α-helix that docks into a hydrophobic surface of the ECD composed of the β1-β2 hairpin loop, loop 2, Tyr^{99}, Pro^{69}, and the Cys^{68}–Cys^{102} disulfide (Fig. 3, *A*, *C*, and *D*). The N terminus of the peptide is oriented such that the 1′–25′ fragment would presumably point toward the transmembrane helical bundle of the receptor. Approximately 1000 $Å^2$ of solvent-accessible surface area is buried at the interface. The interaction is mediated through hydrophobic contacts involving $Leu^{37′}$, $Met^{38′}$, and $Ile^{41′}$ of CRF and a network of hydrogen bonds, primarily at the CRF C terminus (Fig. 3*D*). $Met^{38′}$ appears to provide the most significant hydrophobic interaction as it is completely buried in a small hydrophobic pocket formed by Tyr^{99}, the Cys^{68}–Cys^{102} disulfide, Ile^{51}, Pro^{69}, Phe^{72}, and Tyr^{77}. The C-terminal amide group of CRF forms an intramolecular hydrogen bond between the amide nitrogen and the backbone carbonyl of $Met^{38′}$ stabilizing the α-helical conformation of the peptide. In addition, two intermolecular hydrogen bonds are formed between the C-terminal amide oxygen and nitrogen atoms and the backbone amide nitrogen and carbonyl oxygen of Val^{97}, respectively. These hydrogen bonds provide a clear explanation for the requirement of the C-terminal amide moiety for high affinity binding. The backbone carbonyl of $Glu^{39′}$ is capped by hydrogen bonds with the guanidino group of Arg^{96}. The $Asn^{34′}$ side chain amino group is within hydrogen bonding distance of the hydroxyl of Tyr^{77} and the backbone carbonyl of Phe^{72}. Finally, the side chain amino group of $Gln^{30′}$ is within hydrogen bonding distance of the backbone carbonyl of Tyr^{73}, although the electron density for the amino group is not well defined.

To validate the interactions observed in our crystal structure we performed alanine-scanning mutagenesis of residues in the CRF-(27–41) peptide that contact the ECD and examined the ability of the variant peptides to bind to MBP-CRFR1-ECD using the AlphaScreen assay. We also assayed peptides containing alanine substitutions at positions 39′ and 40′ as controls, as well as a wild-type peptide with a C-terminal carboxylic acid instead of the amide group. The wild-type, unlabeled CRF-(27–41)-NH_2 peptide (100 μM) inhibited >95% of the binding of biotinylated CRF-(12–41)-NH_2 (25 nM) to MBP-CRFR1-ECD-H_6 (25 nM) (Fig. 3*E*). In agreement with the structure, alteration of residues $Leu^{37′}$, $Met^{38′}$, or the C-terminal amide dramatically reduced the ability of the peptides to inhibit the interaction indicating their importance for receptor binding. Alteration of $Glu^{39′}$ or $Ile^{40′}$ had only a minor effect, as expected. Alteration of $Ile^{41′}$ also had only a minor effect, presumably because alanine maintains sufficient hydrophobicity at this position. Surprisingly, alteration of $Asn^{34′}$ did not significantly diminish the ability of the peptides to bind, whereas alteration of $Gln^{30′}$ or $Arg^{35′}$ dramatically reduced binding. It is unclear from our structure why disruption of the $Gln^{30′}$ or $Arg^{35′}$ side chains had such a dramatic effect. The $Arg^{35′}$ side chain does not form any specific intra- or inter-molecular contacts, but it does provide a positive charge sandwiched between the negative charges of $Glu^{39′}$ of CRF and Glu^{104} of the receptor ECD. We cannot exclude the possibility of crystal packing effects hindering the ability of the N-terminal portion of CRF to fully engage loop 2, possibly via interactions mediated by $Gln^{30′}$ and $Arg^{35′}$, but this seems unlikely (supplemental Fig.S2 and S4A). The asparagine residue at position 34′ and hydrophobic residues at positions 37′, 38′, and 41′ are highly conserved in the CRF family of peptides (Fig. 3*F*). The structure and binding assay results taken together suggest that a minimal CRF pharmacophore of $Leu^{37′}$, $Met^{38′}$, $Ile^{41′}$, and the C-terminal amide is required for ECD binding.

We also obtained crystals of the MBP(F94E)-CRFR1-ECD-H_6 protein in complex with a synthetic CRF fragment (residues 27–41). The complex readily crystallized in the tetragonal $P4_12_12$ space group with one MBP-CRFR1-ECD·CRF complex in the asymmetric unit (crystal form III). The structure was solved by MR and refined to an *R* factor of 21.8% (R_{free} factor of 25.2%) at 3.40 Å resolution (Table 1). The refinement at low resolution was aided by the availability of higher resolution MR search models. Electron density was observed for all CRFR1 ECD residues except 104–119 and the His_6 tag, which were excluded from the final model. The F94E alteration in MBP did not have the intended effect, and loop 2 assumed the same conformation observed in crystal form I (Fig. 4*A* and supplemental Fig. S4*B*). Nonetheless, and to our surprise, the CRF peptide was present with clear electron density observed for residues 31′–41′ (Fig. 4, *A* and *B*). CRF forms a straight α-helix that docks into the hydrophobic surface of the ECD, burying ~840 $Å^2$ of the solvent-accessible surface area. The interaction is mediated largely through the same mechanisms observed in the crystal form II structure (Fig. 4*C*). Notably, because of the loop 2 conformation, $Asn^{34′}$ no longer forms the hydrogen bonds observed in crystal form II, consistent with our binding data showing that the $Asn^{34′}$ side chain is dispensable for recep-

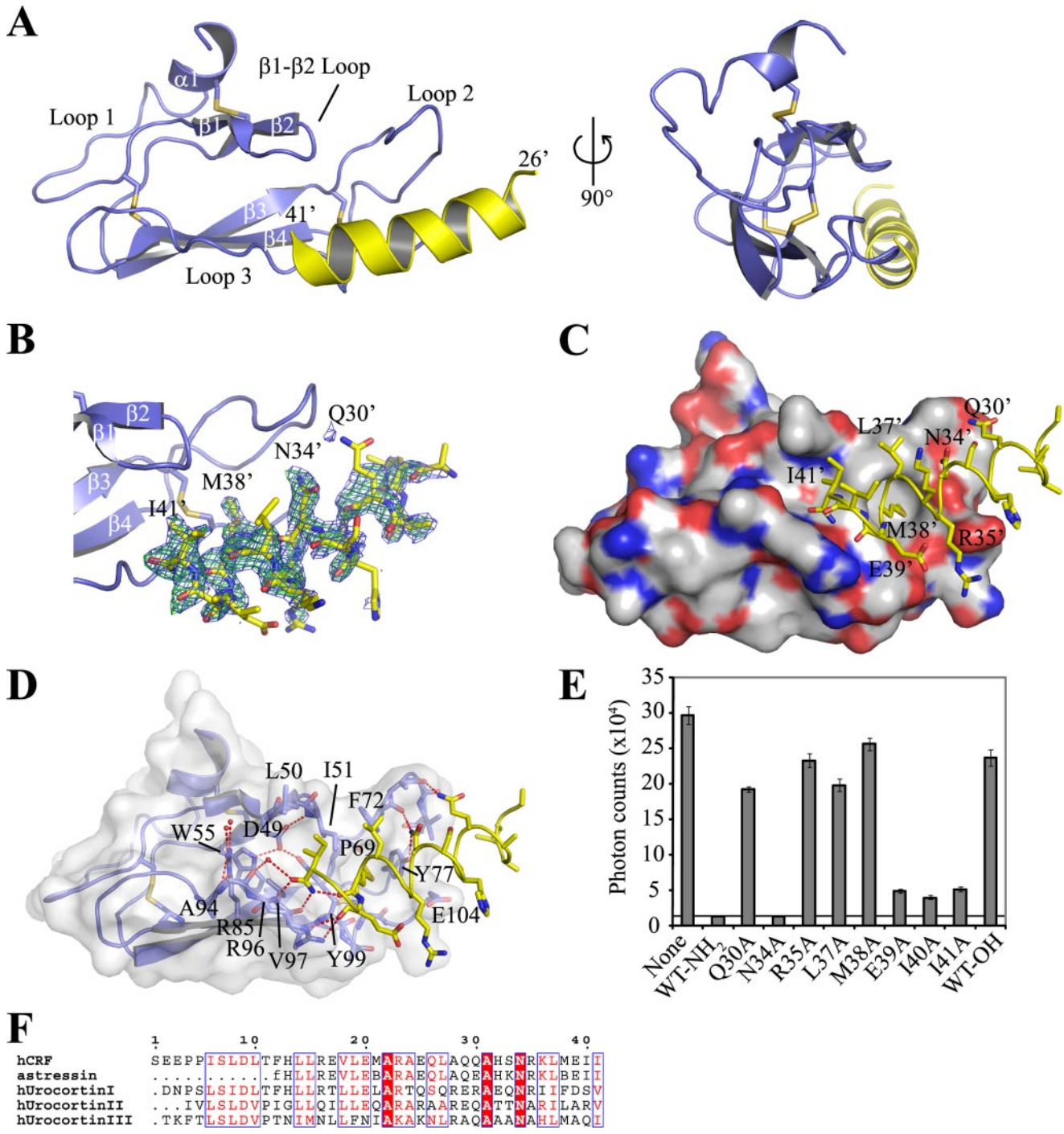

FIGURE 3. **Structural and biochemical analysis of the interaction of CRF with the CRFR1 ECD.** *A*, structure of the CRF-(22–41)-NH_2-bound CRFR1 ECD (crystal form II) presented as a ribbon diagram. The ECD is colored *slate blue* and CRF *yellow*. MBP is not shown for clarity. *B*, electron density maps for CRF. The $2F_o - F_c$ omit map (*blue*) is contoured at 1 σ and the $F_o - F_c$ omit map (*green*) is contoured at 3 σ. The maps were prepared as described under "Experimental Procedures" *C*, molecular surface of the CRFR1 ECD at the peptide-binding site. The surface is colored *gray* for carbon atoms, *blue* for nitrogen atoms, and *red* for oxygen atoms. The CRF peptide is shown as a *yellow coil* with selected side chains as *sticks*. *D*, detail of the interface with the ECD shown as a *slate blue ribbon* diagram covered by a semi-transparent molecular surface, and CRF shown as a *yellow coil*. Selected side chains are shown as *sticks*. Hydrogen bonds are depicted as *red dashes*, and the *red spheres* are water molecules. *E*, AlphaScreen assay assessing the ability of alanine-scan mutants of CRF-(27–41)-NH_2 (100 μM) to compete with the interaction of biotin-CRF-(12–41)-NH_2 (25 nM) and MBP-CRFR1-ECD-H_6 (25 nM). The results shown are the average of triplicate reactions. *F*, amino acid sequence alignment of selected CRF family peptides. Strictly conserved residues are colored *white* on a *red background* and conservative substitutions are colored *red* on a *white background*. The antagonist astressin contains the nonstandard amino acids D-phenylalanine (*f*), and norleucine (*B*).

tor binding (Fig. 3*E*). This structure suggests that specific loop 2 interactions with the peptide are not absolutely required for CRF binding, at least in the context of the isolated ECD, and that the interaction is anchored by the network of hydrogen bonds at the CRF C terminus and the hydrophobic interactions involving $Leu^{37'}$ and $Met^{38'}$. Structural alignment of the crystal form II and III structures support the latter notion, showing that the C terminus of CRF is in a relatively similar position in

the two structures, whereas the position of the N terminus varies significantly (Fig. 4*D*).

Conformational Changes in the CRFR1 ECD Associated with CRF Binding—Crystal structures of the CRFR1 ECD in the ligand-free (crystal form I) and CRF-bound (crystal form II) states afford us the opportunity to analyze conformational changes associated with ligand binding. Changes in loop 2 and the C terminus of the ECD are not interpretable because of the constraints imposed by crystal packing in crystal form I, but other areas of the ECD are amenable to analysis. Alignment of the crystal form I and crystal form II structures shows that the β1-β2 hairpin loop and loop 3 are both shifted inward toward the CRF C terminus in the CRF-bound state as compared with the ligand-free state (Fig. 5). The C-α atoms of Val^{48} and Cys^{54} serve roughly as the pivot points about which the β1-β2 loop is shifted, with the C-α atom of Ile^{51} at the tip of the loop showing the largest shift in position of 1.63 Å from ligand-free to CRF-bound states. Loop 3 is shifted roughly about the pivot points of the C-α atoms of Trp^{93} and Asn^{98}, with the C-α atom of Arg^{96} showing the largest shift of 1.97 Å. In addition, the Arg^{96} side chain rearranges to permit hydrogen bonding with the CRF C terminus. Presumably, the β1-β2 loop conformation is stabilized in the CRF-bound state by hydrophobic interactions with the CRF C terminus, whereas the loop 3 conformation is stabilized by the hydrogen bonds between the C-terminal amide group of CRF and the backbone carbonyl and amide nitrogen of Val^{97}.

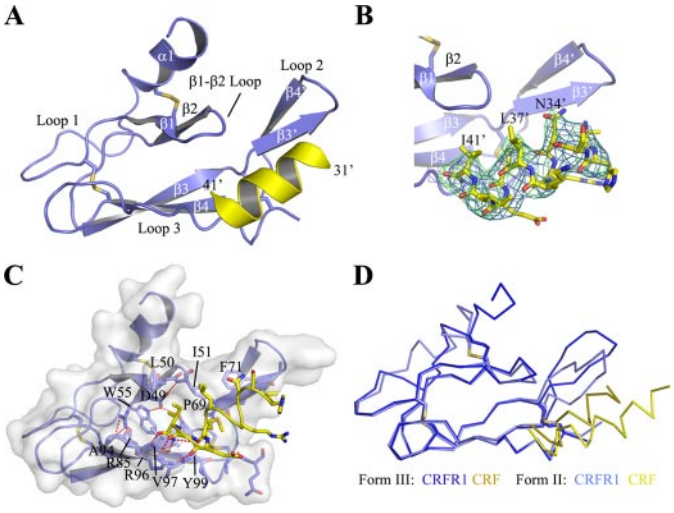

FIGURE 4. **Structure of the CRF-(27–41)-NH_2-bound CRFR1 ECD at 3.4 Å resolution.** *A*, ribbon diagram of the crystal form III complex with the CRFR1 ECD colored *slate blue* and CRF *yellow*. MBP is not shown for clarity. *B*, electron density maps for CRF. The $2F_o - F_c$ omit map (*blue*) is contoured at 1 σ and the $F_o - F_c$ omit map (*green*) is contoured at 3 σ. The maps were prepared as described under "Experimental Procedures." *C*, detail of the interface depicted as in Fig. 3*D*. *D*, alignment of the crystal form II and form III structures. C-α backbone traces are shown with the CRF-(22–41)-NH_2-bound ECD colored *slate blue* and CRF-(22–41)-NH_2 *yellow*. The CRF-(27–41)-NH_2-bound ECD is colored *blue* and CRF-(27–41)-NH_2 *sand*.

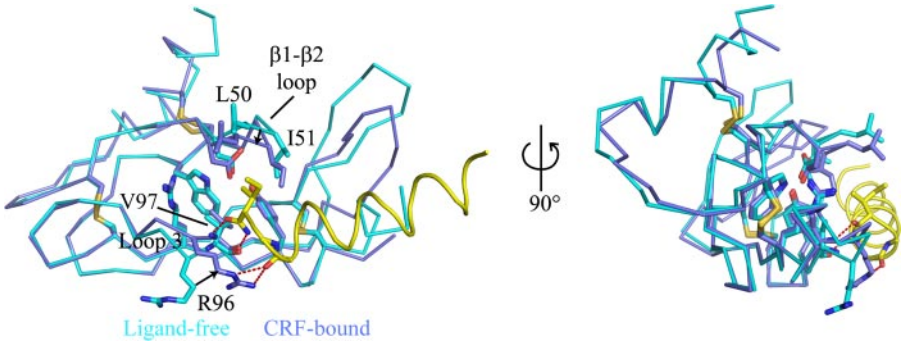

FIGURE 5. **Conformational changes in the CRFR1 ECD associated with CRF binding.** Structural alignment of the ligand-free ECD (crystal form I) and the CRF-(22–41)-NH_2-bound ECD (crystal form II). C-α backbone traces of the ECDs are shown with the ligand-free ECD colored *cyan* and the ligand-bound ECD colored *slate blue*. CRF is shown as a *yellow coil*. Selected side chains are shown as *sticks*, and the *red dashes* depict hydrogen bonds.

DISCUSSION

In this paper, we present three crystal structures of the CRFR1 ECD either in ligand-free or in ligand-bound states. The overall structure of the CRFR1 ECD consists of an α-β-βα fold, resembling other class B GPCR ECDs. The two CRF-bound ECD structures reveal for the first time the detailed molecular mechanisms of the endogenous ligand CRF binding to the CRFR1 ECD, and clearly explain the requirement of the C-terminal amide moiety for high affinity binding and the importance of hydrophobic residues at positions 37′, 38′, and 41′. Comparison of the ligand-free and CRF-bound structures of the CRFR1 ECD revealed conformational changes in the ECD associated with ligand binding. These results provide important insights into peptide binding and selectivity by the CRF receptors.

Surprisingly, the crystal form II and III structures revealed that the CRFR1 ECD is able to accommodate CRF binding in slightly different modes, highlighting the plasticity of the system (Fig. 4*D*). An analysis of crystal packing interactions in the two crystal forms suggests that the crystal form II complex is more representative of the physiologically relevant binding mechanism because loop 2 is unhindered by packing constraints, unlike in crystal form III (supplemental Fig. S4). Despite their differences, the two CRF-bound structures share very similar interactions with the C-terminal portion of the ligand. The interactions observed in the crystal structures were generally supported by our ligand binding data, but a few unexpected results were observed. CRF-(1–41) exhibited higher affinity for the ECD than truncated versions (Fig. 1*D*) even though only the 27–41 fragment interacts with the ECD. This may be due to an increased helical propensity of the full-length peptide as compared with the truncated versions. In addition, the Q30A′ and R35A′ CRF-(27–41) peptides failed to bind the ECD (Fig. 3*E*), despite the absence of significant interactions of these side chains in the crystal structures. A previous study indicated that the $Gln^{30'}$ side chain of ovine CRF was not important for receptor binding (48), whereas conflicting results have been reported for $Arg^{35'}$. The $Arg^{35'}$ side chain was required for receptor binding in the context of ovine CRF (48) or short astressin-based peptides (27) but dispensable in other short astressin-based peptides (28). The role of $Gln^{30'}$ remains unclear, but $Arg^{35'}$ may

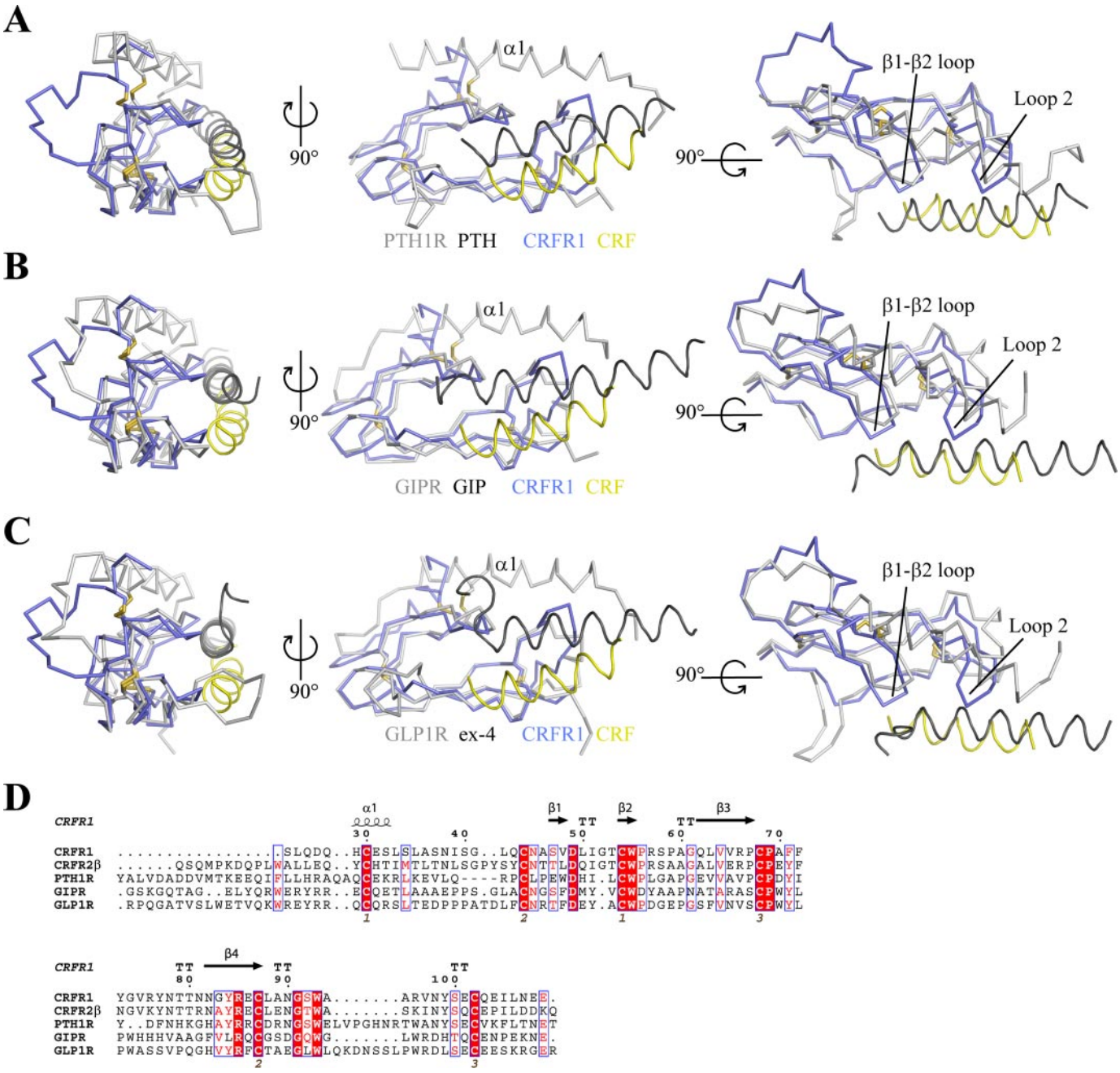

FIGURE 6. **Comparison of the hCRFR1 ECD·CRF complex with the crystal structures of related peptide-class B GPCR ECD complexes.** *A–C*, three views of a structural alignment of the crystal form II CRFR1 ECD·CRF complex with the complexes of PTH (*A*), GIP (*B*), and exendin-4 (*C*) bound to the ECDs of PTH1R (PDB code 3C4M), GIPR (PDB code 2QKH), and GLP1R (PDB code 3C5T), respectively. The ECDs are shown as C-α backbone traces, and the peptides as *coils*. The CRFR1 ECD is colored *slate blue* and CRF *yellow*. The ECDs of PTH1R, GIPR, and GLP1R are colored *light gray,* and their cognate peptide ligands *dark gray*. *D*, amino acid sequence alignment of the human CRFR1 and CRFR2 ECDs with the ECDs of human PTH1R, GIPR, and GLP1R. CRFR1 secondary structure elements are shown at the *top* and the disulfide bond connectivity at the *bottom*. The color scheme is the same as in Fig. 3*F*. PTH1R contains a large insertion in loop 1 that is absent in the other receptors; for clarity, this segment was removed as indicated by *four dashes*. The N-terminal signal peptides are also not shown.

play an important role via electrostatic interactions as discussed later.

The overall binding mode of CRF is similar to that observed for several other peptide ligands with their cognate class B GPCR ECDs (29–32). The amphipathic α-helical peptides interact with a hydrophobic groove on the same face of the ECDs, and the peptides are in the same orientation such that their N-terminal residues would be directed toward the transmembrane helical bundle of the receptor, in agreement with the two-domain model for receptor activation. Despite the overall similarity, the mechanism of CRF binding to the CRFR1 ECD differs in two key aspects from that observed for PTH, GIP, and exendin-4 binding to their cognate receptor ECDs. First, the position of the CRF helix is shifted roughly 5–8 Å as compared with that of PTH, GIP, and exendin-4 (Fig. 6*A–C*). Thus, the CRF binding interface shows little overlap with the PTH, GIP, or exendin-4 binding interfaces when the ECD structures are superimposed. This appears to be due in part to the presence of

an additional residue (Gly^{52}) in the $\beta1$-$\beta2$ loop of CRFR1 and CRFR2 that is not present in the other human class B GPCR ECDs (Fig. 6*D*). This extra residue causes the $\beta1$-$\beta2$ loop to extend further out than in the other receptor ECDs such that it would sterically clash with a peptide located in the same position as PTH, GIP, or exendin-4. In addition, the short N-terminal α-helix of CRFR1 permits loop 2 to project out further than in the other receptor ECDs, which also appears to play a role. Second, the "anchor" point of the interaction of CRF with the CRFR1 ECD is different from that observed for the other peptides. CRF is anchored by the interactions of its C terminus with the $\beta1$-$\beta2$ loop, loop 3, and Tyr^{99} of the ECD. In contrast, PTH, for example, is anchored by interactions of the N-terminal portion of the peptide with loop 2 and the N-terminal α-helix of the PTH1R ECD (31). Thus, by shortening the N-terminal α-helix and extending the $\beta1$-$\beta2$ loop by an extra residue, the CRFR1 ECD has evolved to use a distinct interface for the binding of peptide ligands, suggesting the SCR fold of the class B GPCR ECDs is capable of binding ligands in diverse modes.

The crystal structures of the CRFR1 ECD·peptide complex help to rationalize the NMR data in the literature. Mesleh *et al.* (34) reported the conformation of a minimal astressin-based peptide antagonist bound to the ECD of human CRFR1 determined by NMR methods. Although the structure of the bimolecular complex was not determined, the authors noted the α-helical conformation of the peptide and defined the CRF residues $Met^{38\prime}$, $Ile^{41\prime}$, $Asn^{34\prime}$, and the C-terminal amide as important for receptor binding. These results are in excellent agreement with our structures. The recent NMR structures of the mouse CRFR2β ECD in the ligand-free state and bound to astressin also demonstrated the importance of the same peptide residues for mCRFR2β ECD binding (29). However, the binding mechanism proposed for astressin differs from what we observed for CRF in several aspects. The most striking differences are the overall shift in position of the ligands with respect to the ECD and the loop 2 conformations (Fig. 7*A*–*C*). Astressin contains a cyclic lactam bridge connecting position 30′ and 33′ (Fig. 3*F*) that interacts with the tip of loop 2 in the CRFR2β ECD and could potentially account for the differences. Also, residues that differ between CRFR1 and CRFR2 (Fig. 7, *D* and *E*) could play a role in shifting the astressin position. An intermolecular salt bridge was proposed between $Arg^{35\prime}$ of astressin and Glu^{86} of the CRFR2β ECD, but the CRFR1 ECD contains an alanine (Ala^{70}) at the equivalent position (Fig. 7*E*). In our crystal form II structure, the Ala^{70} side chain is solvent-exposed on the face of loop 2 opposite from the peptide-binding site. The structure differences between CRFR1 and CRFR2β may help to explain the differential ligand selectivity of the two receptors.

Two additional important differences between the CRFR1 and CRFR2β ECD complexes are observed. The most critical difference is the secondary structure of the C-terminal portion of the bound peptides. The NMR structure indicated that the last four residues of astressin form a 3_{10} helix with an intramolecular hydrogen bond between the C-terminal amide nitrogen and the backbone carbonyl of $Glu^{39\prime}$ (29). In contrast, we observed a regular α-helix for CRF with the equivalent hydrogen bond involving the backbone carbonyl of $Met^{38\prime}$. The second important difference concerns the hydrogen bonds formed between the C-terminal amide of the peptide and the receptor. Both the NMR and crystal structures reveal that the C-terminal amide carbonyl oxygen forms a hydrogen bond with the backbone amide nitrogen of the valine in loop 3 (Val^{97} in CRFR1/Val^{113} in mCRFR2β). In addition, the NMR structure suggested an intermolecular hydrogen bond between the C-terminal amide nitrogen of the peptide and the hydroxyl group of Tyr^{115} (Tyr^{99} in CRFR1). However, the crystal structures indicated that this tyrosine plays a structural role in the CRFR1 ECD, forming hydrogen bonds with the conserved aspartate (Asp^{49} in CRFR1/Asp^{65} in mCRFR2β) and a threonine (Thr^{53} in CRFR1/Thr^{69} in mCRFR2β) in the $\beta1$-$\beta2$ loop. Formation of the hydrogen bond proposed by Grace *et al.* (29) would require the breaking of these structural hydrogen bonds. In contrast, we observed a hydrogen bond between the C-terminal amide nitrogen of CRF and the backbone carbonyl of Val^{97}, similar to the pattern of hydrogen bonds we observed for the interaction of the C-terminal amide group of PTH with the PTH1R ECD (31), further supporting our observations for CRF.

Comparison of the ligand-free and CRF-bound structures of the CRFR1 ECD revealed clamp-like conformational changes in the $\beta1$-$\beta2$ loop and loop 3 accompanying ligand binding (Fig. 5). Loop 3 helps to anchor the C terminus of the CRF peptide, and the conformational change of this loop associated with ligand binding also results in the C-terminal capping of the peptide helix dipole. The $\beta1$-$\beta2$ loop is involved in contacts with $Ile^{41\prime}$ and $Met^{38\prime}$ of the peptide. Ligand binding also shifted this loop closer to the peptide, where Ile^{51} at the tip of the loop serves as a key contact residue with the peptide. The NMR structures also suggest that these regions of the mCRFR2β ECD are flexible but become more ordered upon astressin binding (29). These results taken together provide strong evidence for dynamic flexibility in these loop regions and ordering of the loops upon ligand binding. It will be interesting to see if similar conformational changes are observed for other members of the class B GPCR family.

The CRF family of peptides displays distinct specificities for CRFR1 and CRFR2 despite the high degree of similarity in their amino acid sequences (Fig. 3*F*). The affinity of CRF for CRFR1 is 10–40-fold higher than its affinity for CRFR2, whereas UcnII and UcnIII are selective for CRFR2 (7). What is the structural basis for ligand selectivity? Our ligand binding data showed that CRF and UcnI exhibit roughly a 10-fold higher estimated affinity for the CRFR1 ECD than UcnII and UcnIII (Fig. 1*C*), indicating that the ECD alone can discriminate the ligands. Structural and sequence analyses suggest that this selectivity may be determined by CRF residues $Arg^{35\prime}$ and $Glu^{39\prime}$, which are also present in astressin. UcnI has the same $Arg^{35\prime}$ and a similar negatively charged residue $Asp^{39\prime}$, but UcnII and UcnIII have an alanine in both positions (Fig. 3*F*). In our structure, $Arg^{35\prime}$ is sandwiched between $Glu^{39\prime}$ and the CRFR1 residue Glu^{104}, possibly playing an important role in receptor binding through electrostatic interactions (Fig. 7*D*). This conclusion is further sup-

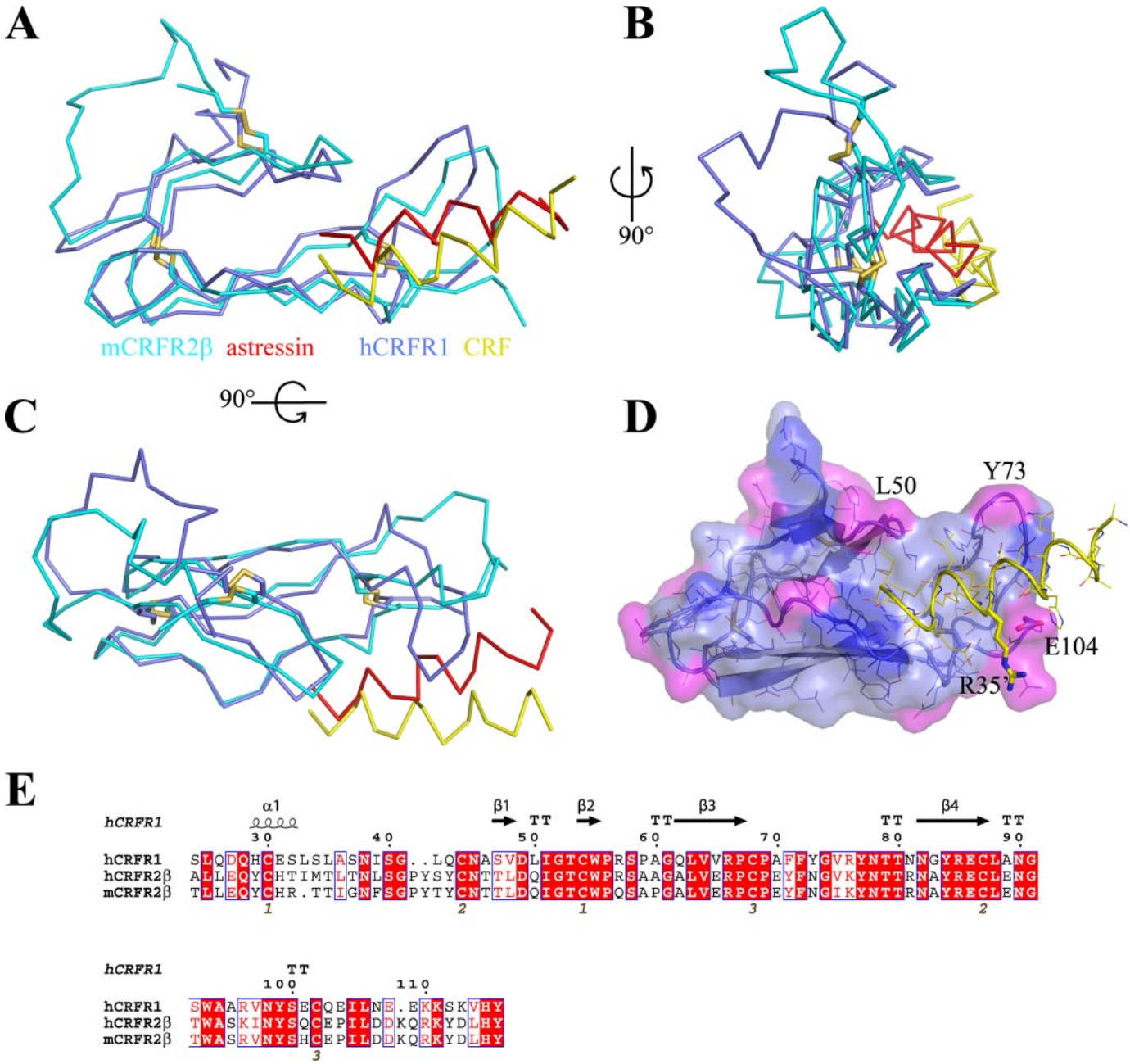

FIGURE 7. **Comparison of the hCRFR1 ECD·CRF complex and the NMR solution structure of the mCRFR2β ECD·astressin complex.** *A–C*, three views of a structural alignment of the crystal form II complex of CRF-(22–41)-NH_2 bound to the hCRFR1 ECD with the NMR solution structure of the mCRFR2β ECD bound to astressin (PDB code 2JND). C-α backbone traces are shown with the CRFR1 ECD·CRF complex colored *slate blue* and *yellow*, respectively, and the CRFR2β ECD·astressin complex colored *cyan* and *red*, respectively. *D*, molecular surface of the CRFR1 ECD from crystal form II colored according to sequence conservation between CRFR1 and CRFR2. The surface is colored *light blue* for residues that are identical, blue for residues that have conservative substitutions, and *magenta* for residues that differ between the two receptors. CRF-(22–41)-NH_2 is shown as a *yellow coil*. *E*, amino acid sequence alignment of the human CRFR1 ECD with the human and mouse CRFR2β ECDs. Secondary structure elements are shown at the *top* and the disulfide bond connectivity at the bottom. The color scheme is the same as in Fig. 3*F*.

ported by the fact that the R35′A mutation in CRF disrupts its binding to the CRFR1 ECD (Fig. 3*E*). Residue Glu^{104} is replaced with a proline in CRFR2, which could explain the selectivity of UcnII and UcnIII for CRFR2 because the $Ala^{35'}$ in these peptides is compatible with the hydrophobic proline. This would explain that the isolated mCRFR2β ECD is also sufficient to discriminate ligands (49). A similar mechanism of ligand selectivity has been proposed based on the mouse CRFR2β ECD NMR structures (29). In addition, ligand selectivity of the full-length receptor can be further refined by additional ligand interactions with the 7-transmembrane helical domain of the receptor (21, 50–52).

Aberrant activation of CRFR1 has been associated with anxiety, depression, and related disorders, and the structures presented here can provide a starting point for the rational design of CRFR1 antagonists targeting the CRFR1 ECD for the treatment of these diseases. The minimal CRF pharmacophore includes residues $Leu^{37'}$, $Met^{38'}$, $Ile^{41'}$, and the C-terminal

amide group, which spans only ~10 Å. The CRFR1 ECD contains a small but deep hydrophobic pocket, where the Met$^{38'}$ side chain of CRF docks. It is tempting to speculate that small molecule compounds, besides peptide antagonists, could be designed to target this pocket and the surrounding surface (Fig. 7*D*). The detailed molecular interactions between CRF and its receptor may thus provide a template for screening small molecule libraries to mimic CRF binding.

Finally, the ability to express, purify, and crystallize the CRFR1 ECD validates the methodology that we previously developed for the PTH1R ECD (31). Importantly, the MBP tag allowed us to crystallize the CRFR1 ECD in both the ligand-bound and ligand-free states, thus overcoming difficulties associated with obtaining crystals of class B GPCR ECDs in their ligand-free state. An additional advantage of using the MBP tag is the ability to alter crystal packing by altering the MBP residues without affecting the fusion targets, thus improving the chance of successful crystallization. The robustness of this method further proves that it is generally useful for biochemical and structural studies of other class B GPCR ECDs, which should greatly facilitate our understanding of ligand recognition by these therapeutically important receptors.

Acknowledgments—We thank S. Anderson and J. Brunzelle for assistance with data collection at sector 21 (LS-CAT) of the Advanced Photon Source. Use of the Advanced Photon Source was supported by the Office of Science of the United States Department of Energy.

REFERENCES

1. Vale, W., Spiess, J., Rivier, C., and Rivier, J. (1981) *Science* **213,** 1394–1397
2. Hsu, S. Y., and Hsueh, A. J. (2001) *Nat. Med.* **7,** 605–611
3. Lewis, K., Li, C., Perrin, M. H., Blount, A., Kunitake, K., Donaldson, C., Vaughan, J., Reyes, T. M., Gulyas, J., Fischer, W., Bilezikjian, L., Rivier, J., Sawchenko, P. E., and Vale, W. W. (2001) *Proc. Natl. Acad. Sci. U. S. A.* **98,** 7570–7575
4. Reyes, T. M., Lewis, K., Perrin, M. H., Kunitake, K. S., Vaughan, J., Arias, C. A., Hogenesch, J. B., Gulyas, J., Rivier, J., Vale, W. W., and Sawchenko, P. E. (2001) *Proc. Natl. Acad. Sci. U. S. A.* **98,** 2843–2848
5. Vaughan, J., Donaldson, C., Bittencourt, J., Perrin, M. H., Lewis, K., Sutton, S., Chan, R., Turnbull, A. V., Lovejoy, D., Rivier, C., Rivier, J., Sawchenko, P. E., and Vale, W. (1995) *Nature* **378,** 287–292
6. Bale, T. L., and Vale, W. W. (2004) *Annu. Rev. Pharmacol. Toxicol.* **44,** 525–557
7. Hauger, R. L., Risbrough, V., Brauns, O., and Dautzenberg, F. M. (2006) *CNS Neurol. Disord. Drug Targets* **5,** 453–479
8. Chen, R., Lewis, K. A., Perrin, M. H., and Vale, W. W. (1993) *Proc. Natl. Acad. Sci. U. S. A.* **90,** 8967–8971
9. Kishimoto, T., Pearse, R. V., 2nd, Lin, C. R., and Rosenfeld, M. G. (1995) *Proc. Natl. Acad. Sci. U. S. A.* **92,** 1108–1112
10. Lovenberg, T. W., Liaw, C. W., Grigoriadis, D. E., Clevenger, W., Chalmers, D. T., De Souza, E. B., and Oltersdorf, T. (1995) *Proc. Natl. Acad. Sci. U. S. A.* **92,** 836–840
11. Perrin, M., Donaldson, C., Chen, R., Blount, A., Berggren, T., Bilezikjian, L., Sawchenko, P., and Vale, W. (1995) *Proc. Natl. Acad. Sci. U. S. A.* **92,** 2969–2973
12. Grammatopoulos, D. K., and Chrousos, G. P. (2002) *Trends Endocrinol. Metab.* **13,** 436–444
13. Fredriksson, R., Lagerstrom, M. C., Lundin, L. G., and Schioth, H. B. (2003) *Mol. Pharmacol.* **63,** 1256–1272
14. Hoare, S. R. (2005) *Drug Discov. Today* **10,** 417–427
15. Dautzenberg, F. M., Wille, S., Lohmann, R., and Spiess, J. (1998) *Proc. Natl. Acad. Sci. U. S. A.* **95,** 4941–4946
16. Perrin, M. H., Sutton, S., Bain, D. L., Berggren, W. T., and Vale, W. W. (1998) *Endocrinology* **139,** 566–570
17. Wille, S., Sydow, S., Palchaudhuri, M. R., Spiess, J., and Dautzenberg, F. M. (1999) *J. Neurochem.* **72,** 388–395
18. Klose, J., Fechner, K., Beyermann, M., Krause, E., Wendt, N., Bienert, M., Rudolph, R., and Rothemund, S. (2005) *Biochemistry* **44,** 1614–1623
19. Perrin, M. H., Fischer, W. H., Kunitake, K. S., Craig, A. G., Koerber, S. C., Cervini, L. A., Rivier, J. E., Groppe, J. C., Greenwald, J., Moller Nielsen, S., and Vale, W. W. (2001) *J. Biol. Chem.* **276,** 31528–31534
20. Nielsen, S. M., Nielsen, L. Z., Hjorth, S. A., Perrin, M. H., and Vale, W. W. (2000) *Proc. Natl. Acad. Sci. U. S. A.* **97,** 10277–10281
21. Hoare, S. R., Sullivan, S. K., Schwarz, D. A., Ling, N., Vale, W. W., Crowe, P. D., and Grigoriadis, D. E. (2004) *Biochemistry* **43,** 3996–4011
22. Rivier, J., Rivier, C., and Vale, W. (1984) *Science* **224,** 889–891
23. Hernandez, J. F., Kornreich, W., Rivier, C., Miranda, A., Yamamoto, G., Andrews, J., Tache, Y., Vale, W., and Rivier, J. (1993) *J. Med. Chem.* **36,** 2860–2867
24. Miranda, A., Koerber, S. C., Gulyas, J., Lahrichi, S. L., Craig, A. G., Corrigan, A., Hagler, A., Rivier, C., Vale, W., and Rivier, J. (1994) *J. Med. Chem.* **37,** 1450–1459
25. Ruhmann, A., Bonk, I., Lin, C. R., Rosenfeld, M. G., and Spiess, J. (1998) *Proc. Natl. Acad. Sci. U. S. A.* **95,** 15264–15269
26. Gulyas, J., Rivier, C., Perrin, M., Koerber, S. C., Sutton, S., Corrigan, A., Lahrichi, S. L., Craig, A. G., Vale, W., and Rivier, J. (1995) *Proc. Natl. Acad. Sci. U. S. A.* **92,** 10575–10579
27. Rijkers, D. T., Kruijtzer, J. A., van Oostenbrugge, M., Ronken, E., den Hartog, J. A., and Liskamp, R. M. (2004) *ChemBioChem* **5,** 340–348
28. Yamada, Y., Mizutani, K., Mizusawa, Y., Hantani, Y., Tanaka, M., Tanaka, Y., Tomimoto, M., Sugawara, M., Imai, N., Yamada, H., Okajima, N., and Haruta, J. (2004) *J. Med. Chem.* **47,** 1075–1078
29. Grace, C. R., Perrin, M. H., Gulyas, J., Digruccio, M. R., Cantle, J. P., Rivier, J. E., Vale, W. W., and Riek, R. (2007) *Proc. Natl. Acad. Sci. U. S. A.* **104,** 4858–4863
30. Parthier, C., Kleinschmidt, M., Neumann, P., Rudolph, R., Manhart, S., Schlenzig, D., Fanghanel, J., Rahfeld, J. U., Demuth, H. U., and Stubbs, M. T. (2007) *Proc. Natl. Acad. Sci. U. S. A.* **104,** 13942–13947
31. Pioszak, A. A., and Xu, H. E. (2008) *Proc. Natl. Acad. Sci. U. S. A.* **105,** 5034–5039
32. Runge, S., Thogersen, H., Madsen, K., Lau, J., and Rudolph, R. (2008) *J. Biol. Chem.* **283,** 11340–11347
33. Sun, C., Song, D., Davis-Taber, R. A., Barrett, L. W., Scott, V. E., Richardson, P. L., Pereda-Lopez, A., Uchic, M. E., Solomon, L. R., Lake, M. R., Walter, K. A., Hajduk, P. J., and Olejniczak, E. T. (2007) *Proc. Natl. Acad. Sci. U. S. A.* **104,** 7875–7880
34. Mesleh, M. F., Shirley, W. A., Heise, C. E., Ling, N., Maki, R. A., and Laura, R. P. (2007) *J. Biol. Chem.* **282,** 6338–6346
35. Bradford, M. M. (1976) *Anal. Biochem.* **72,** 248–254
36. Otwinowski, Z., and Minor, W. (1997) *Methods Enzymol.* **276,** 307–326
37. Collaborative Computational Project, Number 4 (1994) *Acta Crystallogr. Sect. D Biol. Crystallogr.* **50,** 760–763
38. McCoy, A. J., Grosse-Kunstleve, R. W., Adams, P. D., Winn, M. D., Storoni, L. C., and Read, R. J. (2007) *J. Appl. Crystallogr.* **40,** 658–674
39. Murshudov, G. N., Vagin, A. A., and Dodson, E. J. (1997) *Acta Crystallogr. Sect. D Biol. Crystallogr.* **53,** 240–255
40. Jones, T. A., Zou, J. Y., Cowan, S. W., and Kjeldgaard, M. (1991) *Acta Crystallogr.* **47,** 110–119
41. Winn, M. D., Isupov, M. N., and Murshudov, G. N. (2001) *Acta Crystallogr. Sect. D Biol. Crystallogr.* **57,** 122–133
42. Laskowski, R. A., MacArthur, M. W., Moss, D. S., and Thornton, J. M. (1993) *J. Appl. Crystallogr.* **26,** 283–291
43. Thompson, J. D., Higgins, D. G., and Gibson, T. J. (1994) *Nucleic Acids Res.* **22,** 4673–4680
44. Gouet, P., Courcelle, E., Stuart, D. I., and Metoz, F. (1999) *Bioinformatics* (*Oxf.*) **15,** 305–308
45. DeLano, W. (2002) *Py MOL Molecular Graphics System*, Version 0.94, DeLano Scientific, Palo Alto, CA

46. Kleywegt, G. J., and Jones, T. A. (1997) *Methods Enzymol.* **277,** 208–230
47. Perrin, M. H., Grace, C. R., Digruccio, M. R., Fischer, W. H., Maji, S. K., Cantle, J. P., Smith, S., Manning, G., Vale, W. W., and Riek, R. (2007) *J. Biol. Chem.* **282,** 37529–37536
48. Kornreich, W. D., Galyean, R., Hernandez, J. F., Craig, A. G., Donaldson, C. J., Yamamoto, G., Rivier, C., Vale, W., and Rivier, J. (1992) *J. Med. Chem.* **35,** 1870–1876
49. Perrin, M. H., DiGruccio, M. R., Koerber, S. C., Rivier, J. E., Kunitake, K. S., Bain, D. L., Fischer, W. H., and Vale, W. W. (2003) *J. Biol. Chem.* **278,** 15595–15600
50. Dautzenberg, F. M., Kilpatrick, G. J., Wille, S., and Hauger, R. L. (1999) *J. Neurochem.* **73,** 821–829
51. Liaw, C. W., Grigoriadis, D. E., Lorang, M. T., De Souza, E. B., and Maki, R. A. (1997) *Mol. Endocrinol.* **11,** 2048–2053
52. Liaw, C. W., Grigoriadis, D. E., Lovenberg, T. W., De Souza, E. B., and Maki, R. A. (1997) *Mol. Endocrinol.* **11,** 980–985